A Mathematical Model of Imbibition for Two-Phase Flow in Porous Media using a Two-Dimensional Network Model

Kafi Shabbir[1], Oleg Izvekov[1], and Andrey Konyukhov[1]

[1]Moscow Institute of Physics and Technology

September 30, 2023

Abstract

This article is about a network model of two-phase flow in porous media which uses a novel method of distributing different phases in the nodes. In our simulation we measured the saturation of the a phase with respect to time in the region of finer pores. We observed that the saturation rests to an equilibrium value.

Simulation of two-phase flow in porous media has many applications in oil recovery, hydrology, electricity production, etc. Classical continuum models consider permeability to be a function of only saturation. Classical continuum models are unable to explain non-equilibrium effects. Advanced continuum models, such as the Kondaurov model considers permeability to be a function of a non-equilibrium parameter in addition to saturation. In order to better understand the non-equilibrium effects, it is necessary to develop non-continuum models at the scale of the pores, for example a network model.

The objective of our research is to develop a network model which helps us better understand the Kondaurov non-equilibrium parameter.

1 Introduction

Simulation of two-phase flow in porous media has applications in oil recovery, hydrology, electricity production where pressurised water is passed through heated pipes and is transformed into steam, etc. Hence it is important to understand and model two-phase flow in porous medium. [21]

1.1 Classical continuum models

Classical continuum models are widespread and useful. Darcy's Law is an example of classical continuum model. It is given by:

$$q = -\frac{k}{\mu}\nabla p \tag{1}$$

Here, q is the flow rate, k is the permeability, μ is the coefficient of viscosity, and ∇p is the pressure gradient.

The feature of these classical continuum models is that the permeability is only a function of the saturation of one of the phase.

$$k = k(S) \tag{2}$$

Here, k is the permeability as in equation 1, and S is the saturation of one of the phase.

Saturation S is defined as the ratio between the volume occupied by a phase to the total volume of the void. For wetting phase,

$$S_w = \frac{V_w}{V_{void}} \tag{3}$$

Here, V_w is volume occupied by the wetting phase, V_{void} is total volume of the void. For non-wetting phase,

$$S_{nw} = \frac{V_{nw}}{V_{void}} \tag{4}$$

It is clear that,

$$S_w + S_{nw} = 1 \tag{5}$$

In this article we denote S to be the saturation of the wetting phase.

1.2 Advanced continuum models

The classical continuum models are valid as long as the characteristic time of the processes is much longer than the characteristic time of fluid redistribution in the capillary space.

The characteristic time can be longer due to non-equilibrium effects, which occurs when the saturation changes rapidly, or the porous medium is a fractured one with blocks and cracks. In these cases, the assumption that $k = k(S)$ is not sufficient and additional parameters are required.

Various advanced continuum models that take such non-equilibrium effects into account. Models of Hassanizadeh [10] [12] and Barenblatt [4] consider that, the permeability k is a function of the rate of saturation change $\frac{\partial S}{\partial t}$ in addition to the saturation S.

$$k = k(S, \frac{\partial S}{\partial t}) \tag{6}$$

Here,

$$S = S(t) \tag{7}$$

The Kondaurov model [19] considers a special non-equilibrium parameter ξ along with saturation S, which relaxes to an equilibrium value. [18]

$$k = k(S, \xi) \tag{8}$$

This parameter ξ is related to S by the differential equation:

$$\frac{\partial \xi}{\partial t} = \Omega(S, \xi) \tag{9}$$

The objective of our research is to develop a network model which helps us better understand the Kondaurov non-equilibrium parameter ξ.

1.3 Non-continuum models

In order to better understand the non-equilibrium characteristics, it is often necessary to simulate the flow at the scale of pores. Some of the methods of modeling at the scale of pores are, Lattice Boltzmann Method, a direct Navier-Stokes simulation, or a network model. Direct Navier-Stokes simulation provides very accurate results on velocity and pressure distributions, but it is very complicated. Network models are much simpler.

One of the earliest models simulated the flow using a network of electrical resistors [8]. Some of the modern models, such as by Aker et al [2] used an hour glass shaped model of tubes to perform simulation, where the average flow rate was given by the Washburn equation for capillary flow [30]. The disadvantage is that the flow rate must be approximated for cylindrical tube while in their model, the capillary pressure varied depending on its position in the tube.

Our network model uses a novel method of distributing different phases at the nodes. It used only cylindrical tubes, and the flow rate is given by simple equations. In this article we demonstrate the applicability of our model by simulating imbibition.

1.4 Contents of this article

Section 2.1: how we approximated a porous media, so that it can be simulated by a network model.

The summary of how we perform the calculation is:

- Section 2.2: we generate the set of linear equations with pressure as the variables.
- From the calculated pressure in each node, we determine the flow rate in each of the tubes.
- Section 2.3, the phases are distributed in each of the nodes.
- Section 2.4: recombination preserving the center of mass, when there are more then one menisci appears in a tube.

2 Characteristics of the model

2.1 Approximation of a porous medium

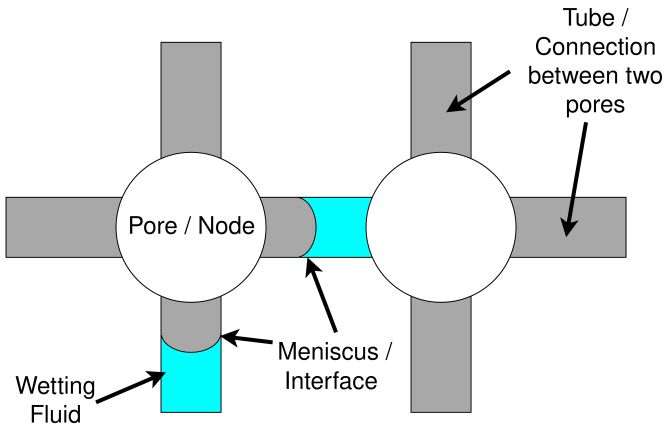

Figure 1: Capillary and pore as tube and node

A porous medium consists of pores, which are connected by capillaries. The pores are represented by nodes, while the capillaries are represented by tubes, as shown in figure 1.

Denotations for our model:

- Our model is two-dimensional
- Each node is connected to 4 other nodes through tubes, shown in figure 2. They may be connected to less than 4 nodes, when they are located on the boundaries.
- The color cyan denotes wetting fluid, while the color gray denotes non-wetting fluid.

Assumptions model:

- The fluids are not compressible.
- The volume of the node is not taken into consideration and is assumed to be zero.
- All tubes are of equal length and cylindrical. The tubes can have different radii.
- The capillary pressure is zero inside the node.
- A tube can have a maximum of 2 menisci.
- During flow, when both cyan and gray fluid enters one node, then the fluids are distributed such that the cyan fluid is distributed first to the thinner tubes.
- During flow, if a tube has more than two meniscus, then there are combined together such that the center of mass of each fluid remains the same.

Note that the assumption of zero volume of node would not change the mixing of different fluids. Let us assume that a node with non-zero volume is filled with gray fluid is invaded by cyan fluid. Since the cyan fluid is distributed first, it immediately reaches the ends of the other tubes connected to the node. The assumption of zero volume of node only affects how the saturation is calculated, never the less it was assumed to be zero to keep the calculations for the flow simple.

2.2 Set of linear equations for a node

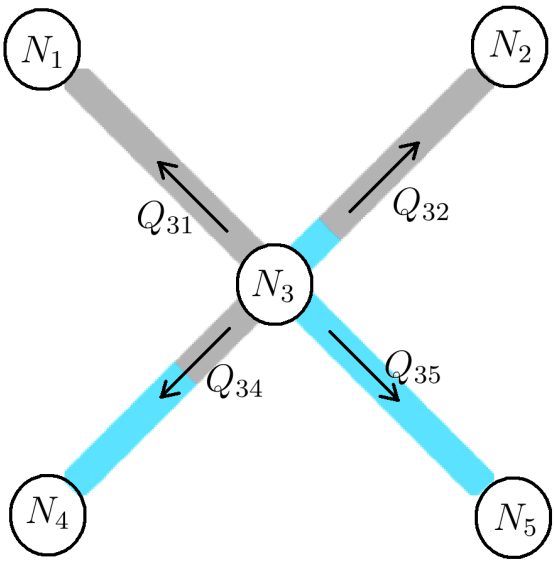

Figure 2: Denotation of flow rates in tubes for one node connected to 5 other nodes

Let the flow rate in a tube be given by,

$$Q_{ij} = A_{ij}\Delta P_{ij} + B_{ij} \tag{10}$$

Here, Q_{ij} is the flow rate form node N_i to node N_i. A_{ij} and B_{ij} are real constants. Here $\Delta P_{ij} = P_i - P_j$, where N_i is kept at a pressure of P_i and N_j at a pressure of P_j. The detailed form is given by equation 38

During simulation, we produce a set of linear equations. We iterate through each node, write equations of flow rates for each tube connected to the node, and equate the sum to zero. For each node, we get one linear equation. For figure2:

$$Q_{3j} = A_{3j}\Delta P_{3j} + B_{3j} \tag{11}$$

Due to the conservation of volume, we have:

$$\sum_k Q_{3k} = 0 \tag{12}$$

Where $k = 1, 2, 4, 5$.

Note that all Q's point outward. The Q's will have different signs in order to preserve the law of conservation of volume.

For fluid flowing out of N_3,

$$Q_{3j} > 0 \tag{13}$$

For fluid flowing into N_3,

$$Q_{3j} < 0 \tag{14}$$

Let us assume that the pressures at all nodes are known, except N_3. Then, the set of linear equations is:

$$\begin{pmatrix} 1 & 0 & 0 & 0 & 0 & P_1 \\ 0 & 1 & 0 & 0 & 0 & P_2 \\ -A_{31} & -A_{32} & (A_{31} + ... + A_{35}) & -A_{34} & -A_{35} & -(B_{31} + ... + B_{35}) \\ 0 & 0 & 0 & 1 & 0 & P_4 \\ 0 & 0 & 0 & 0 & 1 & P_5 \end{pmatrix} \tag{15}$$

2.3 Multi-phase flow in a node

The novelty of our model is how we distribute phases in the nodes. When more than one phase flows into a node, the wetting fluid first enters the tube with the thinner radius. This is to minimize the energy of the system. Below is an example:

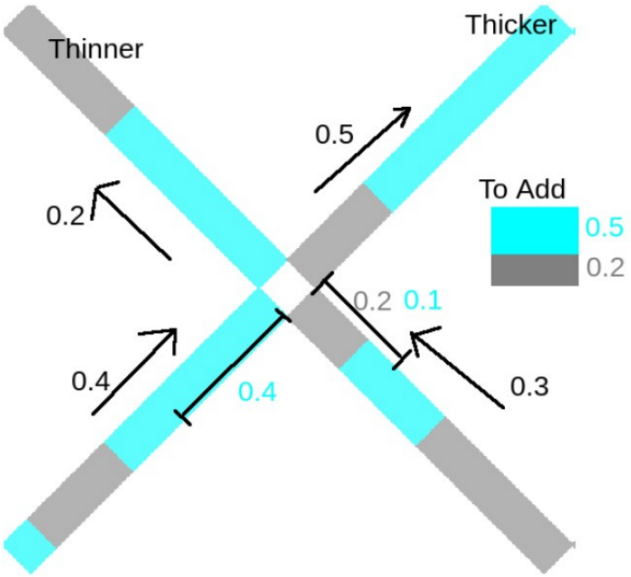

Figure 3: Distribution prediction of different fluids in a node.

In figure 3, let us denote the tubes in the following way:

1. top-left, $tube_1$
2. top-right, $tube_2$
3. bottom-left, $tube_3$
4. bottom-right, $tube_4$

Here, fluid flows from $tube_3$ and $tube_4$ into $tube_1$ and $tube_2$.

From the calculation of flow rates, we determined that $0.7u.v.$ (unit volumes) of fluid enters the node, while $0.7u.v.$ exits the node. They must be equal due to Kirchhoff's law at the node. The total inflow of $0.7u.v.$ consists of $0.4u.v.$ from $tube_3$ and $0.3u.v.$ from $tube_4$. The outflow consists of $0.2u.v.$ into $tube_1$, and $0.5u.v.$ into $tube_2$.

Step-1, we calculate the sum of volume of each type of fluid flowing into the node. Here, $tube_3$ provides $0.4u.v.$ of cyan fluid, while $tube_4$ provides $0.1u.v.$ of cyan fluid and $0.2u.v.$ of gray fluid. Summing we obtain $0.5u.v.$ of cyan fluid and $0.2u.v.$ of gray fluid, which needs to be distributed to the outflow tubes.

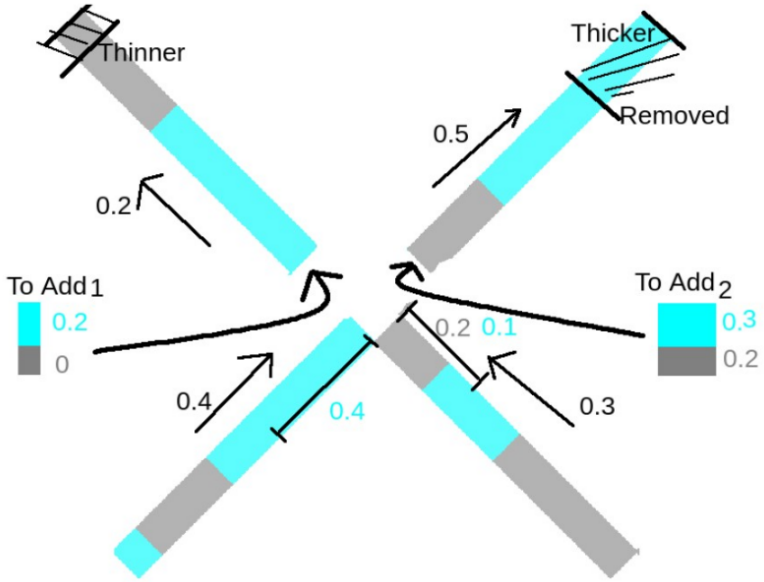

Figure 4: Adding wetting phase to the thinner tube first.

Step-2, we allocate this $0.5u.V.$ of cyan fluid first into the thinner tube. The thinner $tube_1$ takes in $0.2u.V.$. This allocation space is entirely filled by $0.2u.V.$ of cyan fluid. Then for the thicker tube, we need to insert $0.5u.V.$ of fluid into it. $0.3u.V.$ of cyan fluid is inserted first then $0.2u.V.$ of gray fluid.

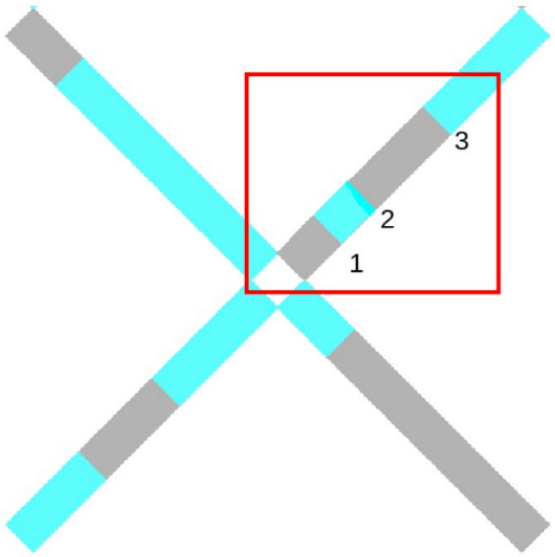

Figure 5: Final tube configuration with 3 menisci.

In figure 5, $tube_1$ retains the only meniscus because the end connected to the node initially contained cyan fluid, and we introduced $0.2u.V.$ of more cyan fluid. The single meniscus was just displaced upwards.

However, in $tube_2$, gray fluid was on the end of the tube connected to the node. We added $0.3u.V.$ of cyan and $0.2u.V.$ of gray fluid. Since the cyan fluid entered the thicker tube first, we end up with 3 menisci.

2.4 Recombination

Our data structure was constrained to only allow the case for a maximum of two menisci in a tube. However, we see that in figure 5 that there is possibility of more than 2 menisci occurring after distribution. We show the cases of distributing fluid in the nodes, which results in more than 2 menisci.

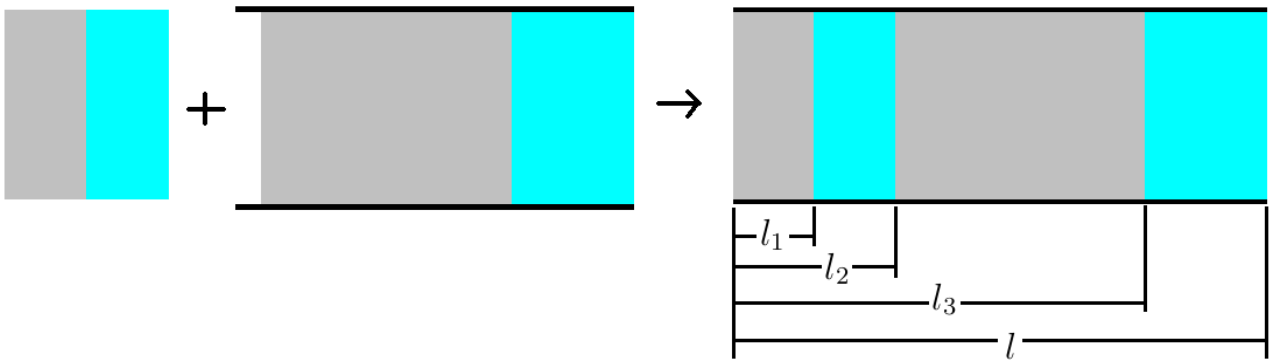

Figure 6: Recombination of 3 menisci

In figure 6 we have a known amount of cyan and gray fluid which we need to insert into the tube. The tube which already consists of both the fluids. The flow is from left to right, so we insert the incoming fluids on the left end of the tube. Note that a block of cyan fluid always ends up in the center as it enters the tube first.

Let l_i denote the location of a meniscus. Since the tube is cylinder, the mass is simply proportional to the length they occupy in the tube, they are given by:

$$m_1 = l_2 - l_1 \tag{16}$$

$$m_2 = l - l_3 \tag{17}$$

Their respective center of masses d_1 and d_2 are given by:

$$d_1 = \frac{l_1 + l_2}{2} \tag{18}$$

$$d_2 = \frac{(l_3 + l)}{2} \tag{19}$$

The center of mass of the cyan fluid in the tube is then given by:

$$d = \frac{m_1 d_1 + m_2 d_2}{m} \tag{20}$$

Here,

$$m = m_1 + m_2 \tag{21}$$

We do not change the proportion of fluids in a tube during recombination. Therefore, it can be shown that if we recombine the fluids in a tube such that the center of mass of one of the fluid remained the same, then the center of mass of the other fluid will also remain the same.

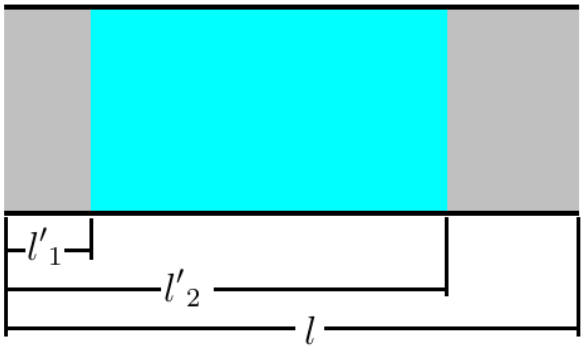

Figure 7: After recombination

Let l'_i denote the position of meniscus after recombination.

$$l'_1 = d - \frac{m}{2} \tag{22}$$

$$l'_2 = d + \frac{m}{2} \tag{23}$$

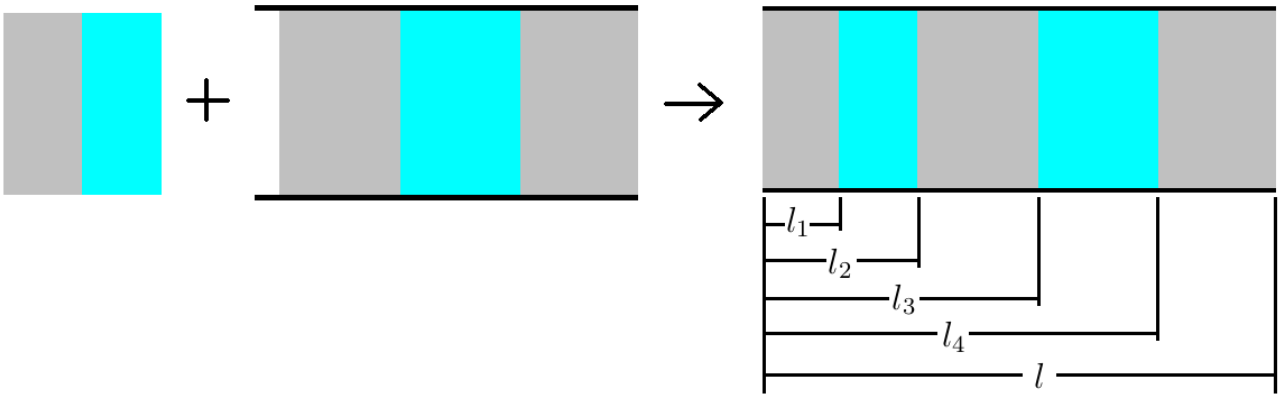

Figure 8: Recombination of 4 menisci

When there are 4 menisci, we repeat the same process, except here:

$$m_2 = l_4 - l_3 \tag{24}$$

And

$$d_2 = \frac{(l_3 + l_4)}{2} \tag{25}$$

3 Methods of calculations

3.1 Flow rate in a tube with one meniscus

At first we derive the equation for flow rate when there is one meniscus present in a tube, then we generalize the case for n menisci. The flow rate of a viscous fluid through a thin tube is given by the Hagen–Poiseuille equation:

$$Q = \frac{\pi}{8\mu}\frac{\Delta P}{l}R^4 \tag{26}$$

Here, Q is the volumetric flow rate in $[m^3/s]$, ΔP is the pressure difference between the ends of the tube, μ is the viscosity in $[kg/m.s]$, l is the length of the tube, R is the radius of the tube.

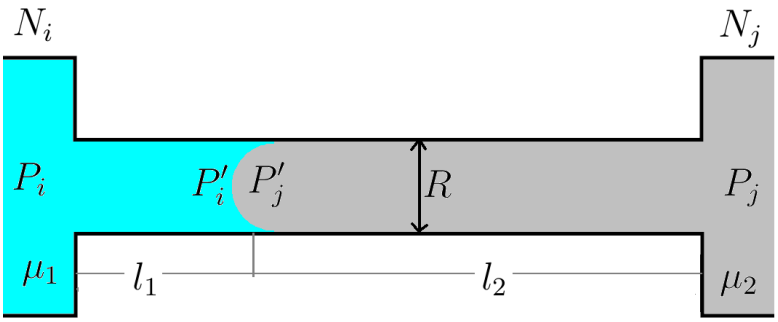

Figure 9: Orientation of the meniscus, the convex side contains wetting fluid while the concave side contains non-wetting fluid.

In figure 9, node N_i kept at a pressure of P_i, and is filled with a wetting fluid of viscosity μ_1. Node N_j kept at a pressure of P_j is filled with a non-wetting fluid of viscosity μ_2. It is evident that the pressure on the convex size or on the part of the wetting fluid is lower.

$$P_i' < P_j' \tag{27}$$

The pressure jump is given by:

$$P_j' - P_i' = \frac{2\sigma}{R} \tag{28}$$

Here, σ is the coefficient of surface tension in $[Pa.m]$ or $[kg/s]$.

Separating figure 9 into two tubes of lengths l_1 and l_2, containing fluids of viscosity μ_1 and μ_2. The flow rates of the tubes, from equation 26 are given by:

$$Q = \frac{\pi}{8\mu_1}\frac{P_i - P_i^{'}}{l_1}R^4 \tag{29}$$

$$Q = \frac{\pi}{8\mu_2}\frac{P_j^{'} - P_j}{l_2}R^4 \tag{30}$$

Due to the law of conservation of volume, the flow rates are equal. Adding the equations 29 and :

$$Q(\mu_1 l_1 + \mu_2 l_2) = \frac{\pi}{8}R^4(P_i - P_j + P_j^{'} - P_i^{'}) \tag{31}$$

Substituting the equation 28 about capillary pressure,

$$Q = \frac{\pi R^4}{8Ml}\left(\Delta P_{ij} + \frac{2\sigma}{R}\right) \tag{32}$$

Here,

$$\Delta P_{ij} = P_i - P_j \tag{33}$$

And M is the viscosity parameter:

$$M = \sum_k \mu_k \frac{l_k}{l} \tag{34}$$

Note that the viscosity parameter, remains the same for any number of menisci present in a tube.

3.2 Flow rate in a tube with multiple menisci

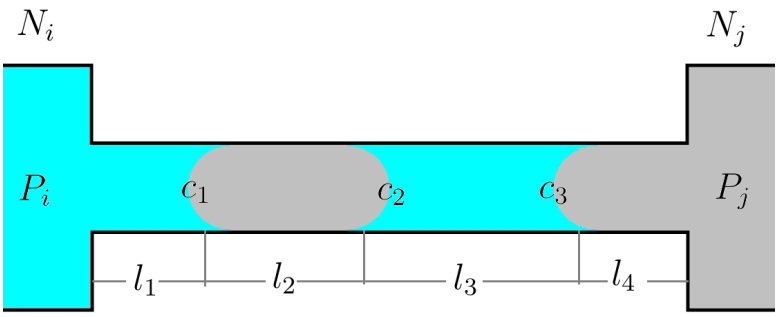

Figure 10: Capillary pressure contribution, $s = 1$

Let the capillary pressures be denoted by the following:

$$c_1 = -c_2 = c_3 = \frac{2\sigma}{R} \tag{35}$$

Then for figure 10, the flow rate is given by:

$$Q = \frac{\pi R^4}{8Ml} \left(\Delta P_{ij} + c_1 + c_2 + c_3\right) \tag{36}$$

$$Q = \frac{\pi R^4}{8Ml} \left(\Delta P_{ij} + \sum_k c_k\right) \tag{37}$$

Flow rate for an arbitrary number of meniscus for a cylindrical tube, is given by:

$$\boxed{Q = \frac{\pi R^4}{8Ml} \left(\Delta P_{ij} + \frac{2s\sigma}{R}\right)} \tag{38}$$

Where,

$$s(d, n_{mns}) = \begin{cases} -1, & n_{mns} = 1,\ d \text{ points away from } N_i \\ 0, & n_{mns} = 0,\ 2 \\ +1, & n_{mns} = 1,\ d \text{ points towards } N_i \end{cases} \tag{39}$$

Here,

- d, the direction the convex side of the meniscus points towards

- n_{mns}, the number of meniscus in a tube

In our model, the data structure does not accommodate more than 2 meniscus in a tube, hence in the definition of s, $n_{mns} \leq 2$. Shown that, for figure 10, 11, and 12, s is 1, -1, and 0 respectively.

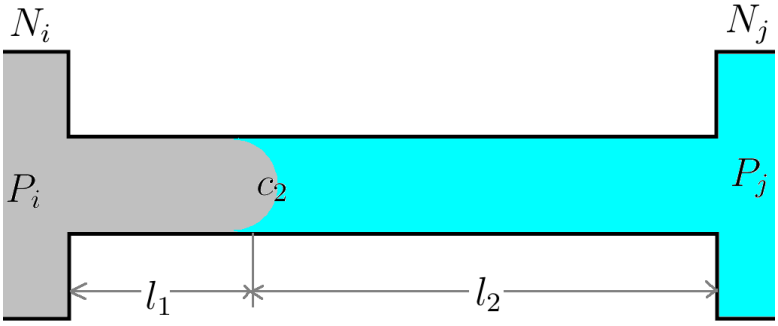

Figure 11: Capillary pressure contribution, $s = -1$

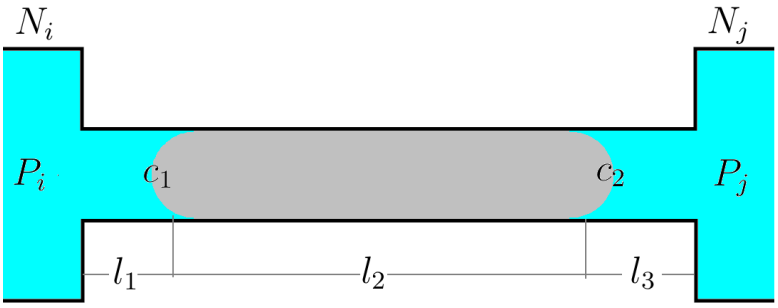

Figure 12: Capillary pressure contribution, $s = 0$

3.3 Flow rate and velocity

Therefore, in equation 10, we get:

$$A_{ij} = \frac{\pi R_{ij}^4}{8 M_{ij} l} \Delta P_{ij} \tag{40}$$

$$B_{ij} = \frac{\pi R_{ij}^4}{8 M_{ij} l} \frac{2 s_{ij} \sigma}{R_{ij}} \tag{41}$$

Here, note that:

$$R_{ij} = Rji \tag{42}$$

$$M_{ij} = Mji \tag{43}$$

$$P_{ij} = -Pji \tag{44}$$

$$s_{ij} = -sji \tag{45}$$

When the pressures are known in each nodes, the velocity is determined by:

$$v_{ij} = \frac{Q_{ij}}{\pi R_{ij}^2} \frac{R_{ij}^2}{8 M_{ij} l} \left(\Delta P_{ij} + \frac{2 s_{ij} \sigma}{R_{ij}} \right) \tag{46}$$

[COMMENT: Not satisfied, in Pousielle's flow, the flow on the boundary is 0, and maximum in the center, how do we reason for selecting $v = Q/\pi R^2$?]

3.4 Algorithm for computation

1. **Input constants:** μ_1, μ_2, l, σ.
2. **Input files:** radius and menisci distribution.
3. **Random radius:** add very small random values to the radius distribution, so that there is an unique way of distributing fluids into the tubes.
4. **Create 0 matrix:** M_{ij} of n rows and $n+1$ columns, where n is the number of nodes in our system, this matrix will be used to determine the pressures in each node.
5. **Time passed:** set $t = 0$.
6. **Main loop:** until a certain saturation S is reached in a given region, or for a fixed number of frames:
   (a) **Generate linear equations:** iterate for every N_i, $1 \leq i \leq n$:
      i. **Generate connections:** the list of nodes N_j and tubes b_{ij}, which are connected to N_i.
      ii. **Iterate connections:** for each node N_j connected to N_i, this generates one row of M_{ij}:
         A. R_{ij} is obtained from radius distribution. M_{ij}, s_{ij} is calculated from current meniscus configuration of b_{ij}.
         B. Using R_{ij}, M_{ij}, s_{ij}, and other constants, calculate A_{ij} and B_{ij} according to equations 40 and 41.
         C. Perform the following modifications to M_{ij}:
         D. $M_{ii} = M_{ii} + A_{ii}$
         E. $M_{ij} = M_{ij} - A_{ij}$
         F. $M_{i,n+1} = M_{i,n+1} - B_{ij}$
   (b) Calculate pressures: solve M_{ij}. Gaussian-elimination was used for the results of simulations shown in this article.
   (c) **Calculate velocity:** from the pressures calculated in each node, determine the velocity in each tube using equation 46
   (d) **Calculate time step:** the time step for integration $\Delta t = min(\Delta t_{ij})$, here $\Delta t_{ij} = c_t minl/v_{ij}$ for each tube b_{ij}. $c_t = 0.1$ was used for the simulations.
   (e) **Calculate volume displacement**, the volume displaced in each tube is determined by, $V_{ij} = v_{ij} \Delta t$.
   (f) **Store distribution:** iterate through each tube, and store how much of which fluid enters into the node towards which there is positive velocity.

(g) **Distribute fluids:** iterate through all the nodes, and for each node N_i:

i. determine which tubes take away fluid from N_i.

ii. distribute the wetting and non-wetting fluids according to the algorithm described in 2.3.

iii. recombine when a tube has more than 2 menisci, according to 2.4

(h) **Save a picture** of the current configuration.

(i) Calculate the new saturation S.

(j) Update time, $t = t + \Delta t$.

(k) Add a point to the plot, (t, S).

7. A video file is generated.

3.5 Possible Cases of Errors

3.5.1 Initial configuration for flow to start

The flow did not start when all the meniscus were located inside the nodes. Because in our model we assumed that there is not capillary pressure in the nodes. To overcome this, the meniscus were made to be situated inside the tubes.

3.5.2 Case of all meniscus located in the thick tubes

The solution of linear equation were such that, the capillary force balanced out the pressure gradient. The pressure was much higher outside in the thick tubes than in the thin tubes. Whether this was caused by error in the process of solving the linear equation or due to the initial setup, needs to be checked again. Error is, that it is impossible to determine whether the coefficient during the process of gauss elimination is zero or not. Because of the way how floating point numbers are handled by the CPU, 0 is often seen as a small number.

3.6 Simple tests for our model

3.6.1 Filtration

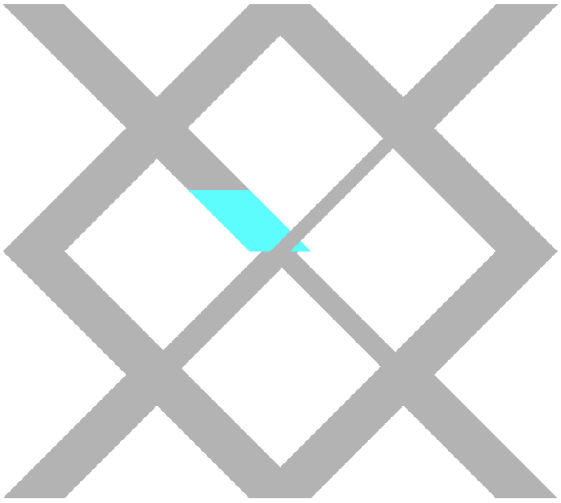

Figure 13: Initial position of wetting fluid

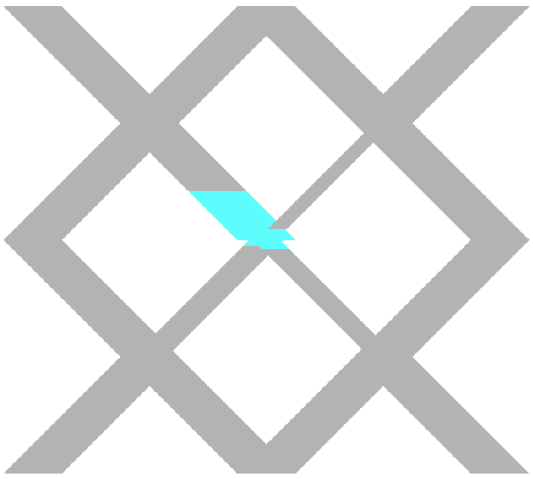

Figure 14: The wetting fluid chose to move to the tubes with thinner radius.

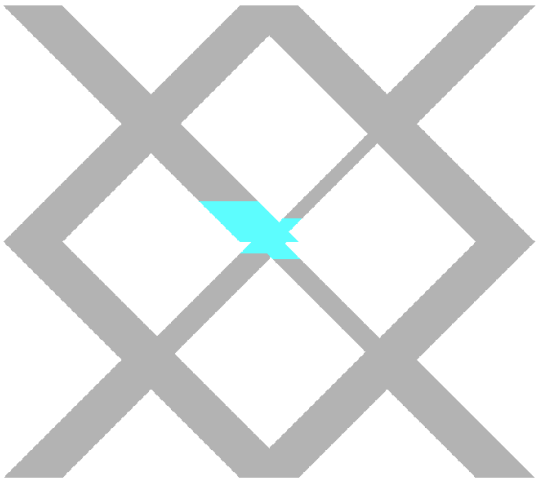

Figure 15: The flow accelerates as more fluid is in the thinner radius, here viscosity of the wetting fluid is higher.

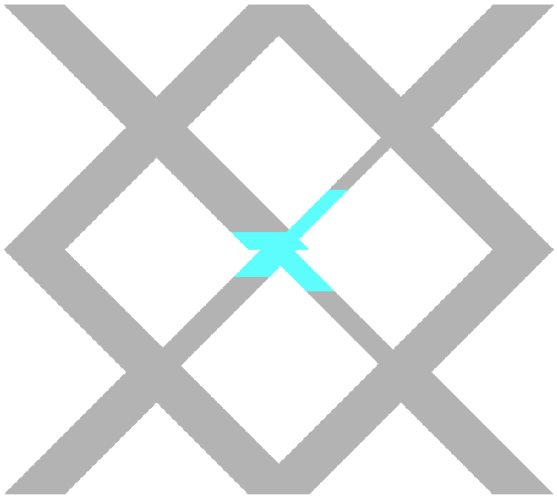

Figure 16

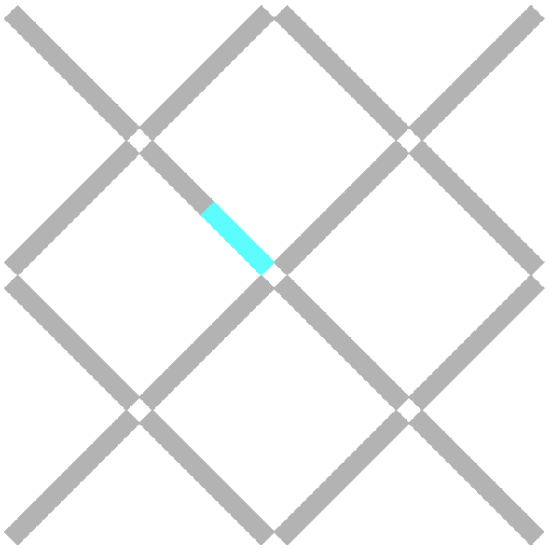

Figure 17: The same flow without plotting the radius thickness for clarity.

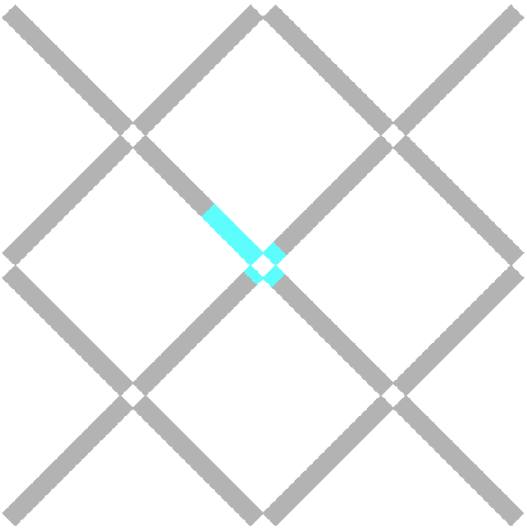

Figure 18

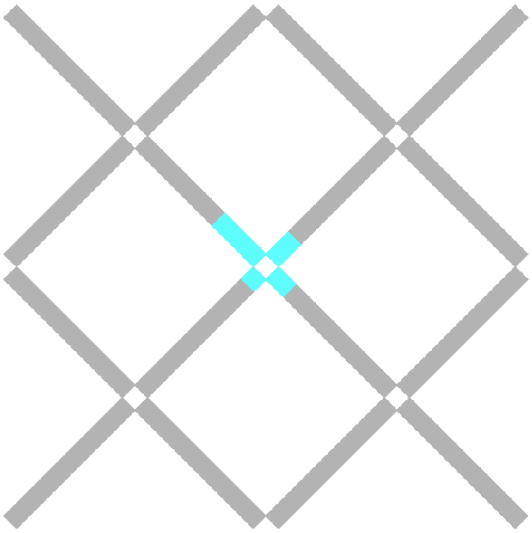

Figure 19

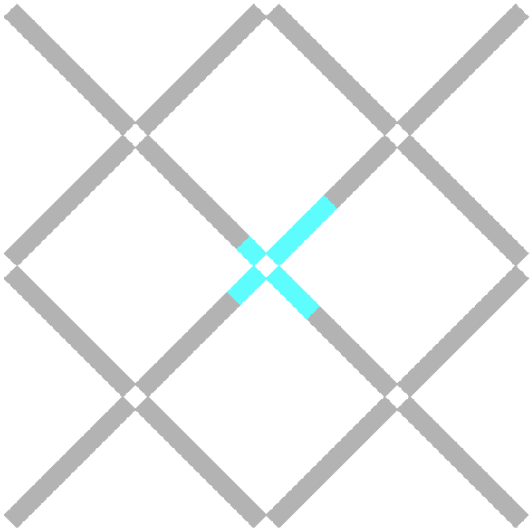

Figure 20

3.6.2 Displacement

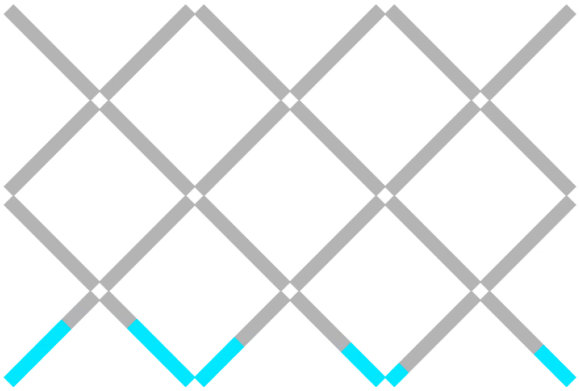

Figure 21: Our model is initially set up such that the wetting fluid is low in saturation and is confined to the bottom of our network. A higher pressure is fixed for all nodes at the bottom layer, while a low pressure is fixed for the top row.

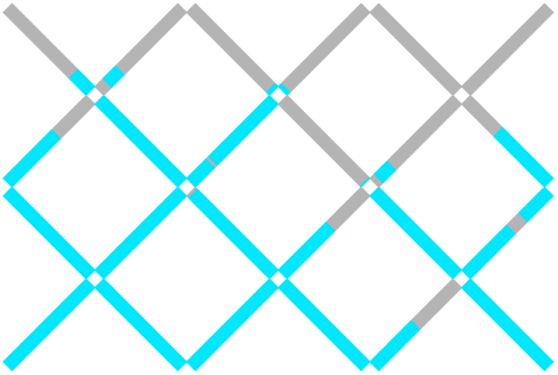

Figure 22: In all nodes, law of conservation of volume is applied, since mass is conserved and the phases are non-compressible. However for the bottom layer of nodes, the wetting fluid is injected as much required according to the sum of flow rates determined in the tubes connected to those nodes, while from the top layer of nodes a fluid is removed.

3.7 Initial conditions for the main experiment - imhibition

- Closed boundaries.
- The aim of this simulation is observe the movement of wettable fluid (blue) from the region of thicker tube to the thinner tube.
- The saturation of each phase is measured in the region of thinner tubes.
- All boundaries are closed, the saturation of a phase for the whole system remains constant in time.
- The radius in the outer region is three times larger.
- The radius of the outer region is 3 times larger than inner.
- We plan to observe, that the invasion slows down and possibly oscillates, it is due to the meniscus in the inner region being ineffective to suck more blue fluid as most tubes have two meniscus. In our algorithm, tubes with two meniscus have a zero net pressure.

- EDIT Wetting(cyan) fluid into the region which contains thinner radius. The flow accelerates because, for a corner initially there are 3 meniscus, it multiplies into 3 when the meniscus reaches the node. The corner where the meniscus reaches the node late is pushed back because of the excessive pressures from the other corners.

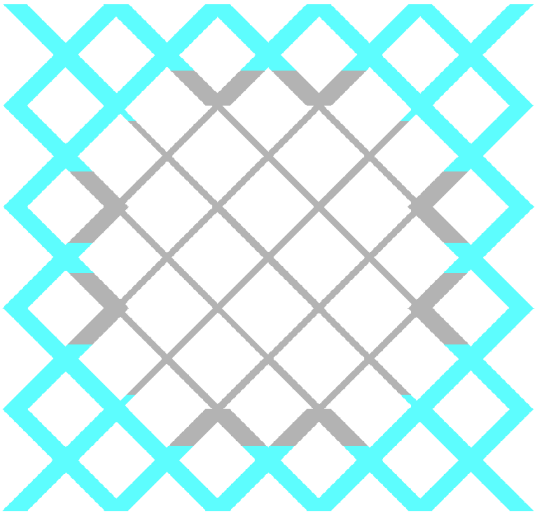

Figure 23: Initial setup, outer radius is 3 times larger than inner.

3.8 Linear equations in case of infinitely many solutions

It is possible to calculate the pressures at each node, if the pressures are known on the edges. However when we want to model imhibition, the boundaries are closed and the total volume of a phase remains the same.

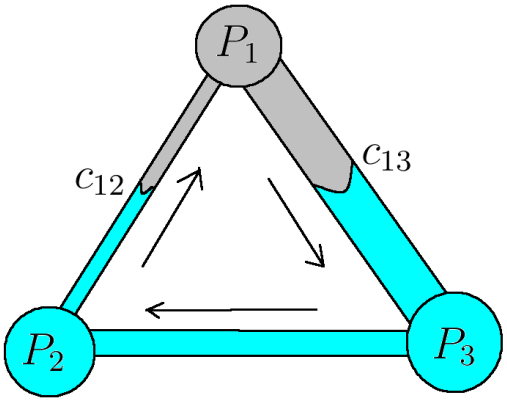

Figure 24: Case of of infinitely many solutions

Let the flow rates be given by:

$$q_{ij} = k_{ij}\Delta P + c_{ij} \tag{47}$$

For N_1:

$$q_{12} = k_{12}(P_1 - P_2) + c_{12}$$
$$q_{13} = k_{13}(P_1 - P_3) + c_{13}$$

Since:

$$q_{12} + q_{13} = 0$$

$$(k_{12} + k_{13})P_1 - k_{12}P_2 - k_{13}P_3 = -c_{12} - c_{13}$$

Then for each node we obtain the following matrix:

$$\begin{pmatrix} (k_{12}+k_{13}) & -k_{12} & -k_{13} & -c_{12}-c_{13} \\ -k_{21} & (k_{21}+k_{23}) & -k_{23} & -c_{21}-c_{23} \\ -k_{31} & -k_{32} & (k_{31}+k_{32}) & -c_{31}-c_{32} \end{pmatrix}$$

Note that:

$$k_{ij} = k_{ji}$$

$$c_{ij} = -c_{ji}$$

Hence the sum of each column of this matrix is zero.

By $R_3 = R_3 + R_1 + R_2$:

$$\begin{pmatrix} (k_{12}+k_{13}) & -k_{12} & -k_{13} & -c_{12}-c_{13} \\ -k_{21} & (k_{21}+k_{23}) & -k_{23} & -c_{21}-c_{23} \\ 0 & 0 & 0 & 0 \end{pmatrix}$$

This is solved by adding a constant a to one of the column of the matrix for each rows. In our model the centre was chosen to be the zero of pressure. Changing this point does not change the flow rates or the nature of flows.

$$\begin{pmatrix} (k_{12}+k_{13}) & -k_{12} & -k_{13}+a & -c_{12}-c_{13} \\ -k_{21} & (k_{21}+k_{23}) & -k_{23}+a & -c_{21}-c_{23} \\ -k_{31} & -k_{32} & (k_{31}+k_{32})+a & -c_{31}-c_{32} \end{pmatrix}$$

After $R_3 = R_3 + R_1 + R_2$:

$$\begin{pmatrix} (k_{12}+k_{13}) & -k_{12} & -k_{13}+a & -c_{12}-c_{13} \\ -k_{21} & (k_{21}+k_{23}) & -k_{23}+a & -c_{21}-c_{23} \\ 0 & 0 & 3a & 0 \end{pmatrix}$$

$$3aP_3 = 0$$

The solutions exists only if $P_3 = 0$.

4 Simulation and results

4.1 Figures

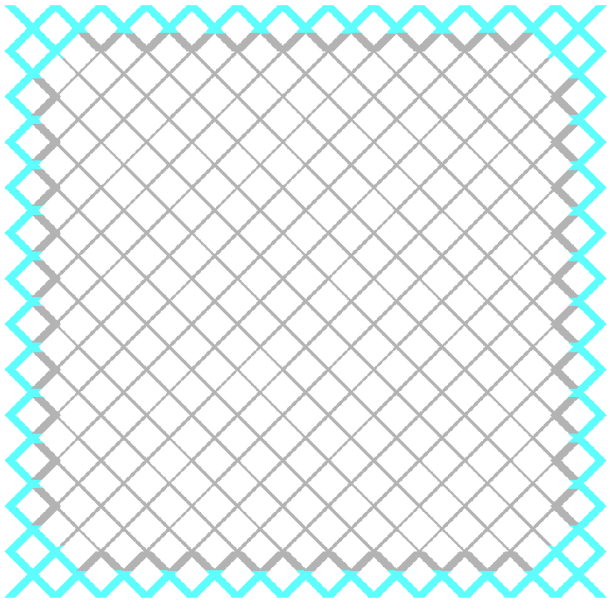

Figure 25: Initial setup

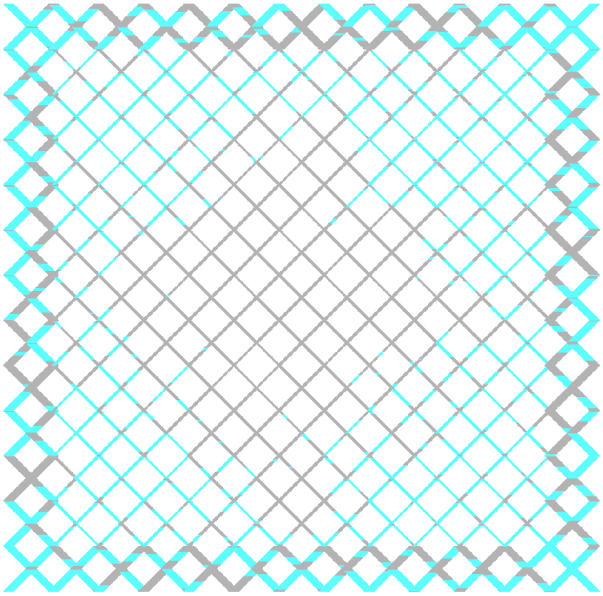

Figure 26: Flow accelerating

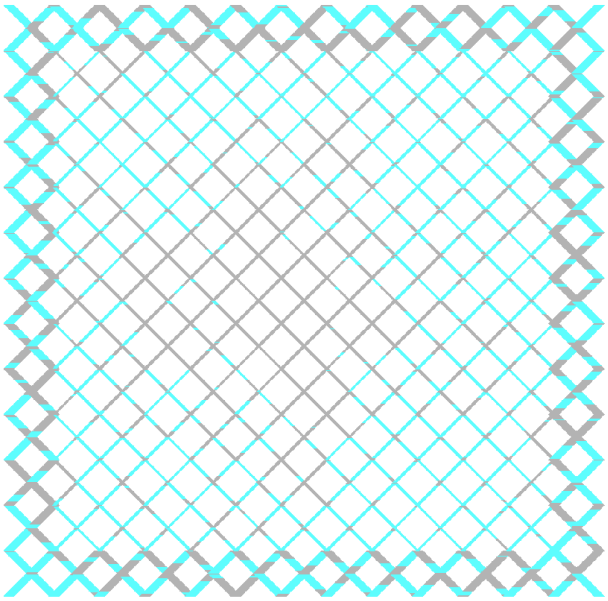

Figure 27: Final

4.2 Plot

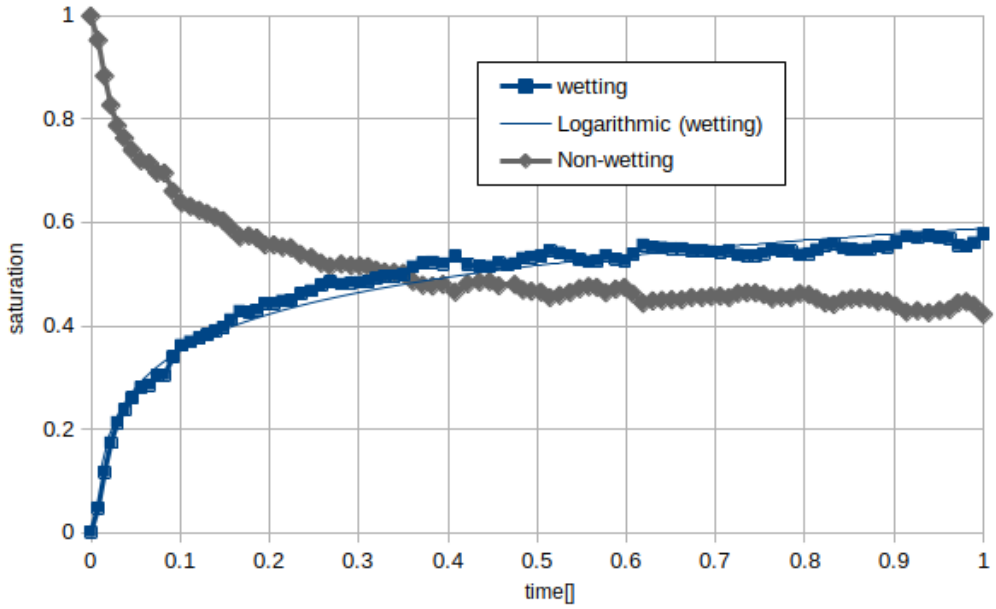

Figure 28: Plot of saturation of blue fluid in the region of thinner radius with respect to dimensionless time.

Changing the ratio of viscosity affects the rate of displacement in the presence of pressure gradient, however in the case of inbibition significant differences were not observed.

4.3 Discussion

1. Calculation was done for 20,000 steps.
2. Plot for every 200 frames.
3. Equal volumes of each phases.

4. The saturation for wetting fluid is 0.57 for the inner region, which is very close the previous simulation for 10x10.
5. It is clear that the relaxation parameter is present as the saturation converges to an equilibrium value.
6. For the simulations the length of each tube was taken to be unity and only the ratio of viscosity was used in equation **??**, since these values do not change the geometry of the flow and change only the scale of time. Dimensionless value of time was used.
7. Logarithmic dependence was observed [EDIT-ADD equations determine the physical meaning of the non equilibrium parameter, and the scope of its applicability.]

5 Conclusions

1. The saturation of a phase in the inner region of the porous body tends to an equilibrium value.
2. The method of distributing fluid such the wetting fluid first goes to the tube with the thinner radius and calculating the flow rate using the modified Poiseuille equation is valid for explaining relaxation phenomena.
3. This algorithm can be extended to the case where there are more than 4 tubes connected to a node, since for two phase flow into a node case, we distribute in an ascending order of radii, in our model it is distributed to a maximum number to two tubes, but for hexagonal model it can be 4. We only need to update the function which produces the connections. The same model can be used for a 3-dimensional case, where one surface has higher pressure than the opposite surface which has a lower pressure, it is to be used in order to more accurately represent the porous body.
4. Model of reasonable size can be simulated using Gaussian-elimination, which is more accurate than iterative methods.
5. The total volume for each phase for the whole system remains the same with the accuracy of 10^{-9}. Use of double is recommended instead of float.

6 Acknowledgments

This project was supported by Russian Science Foundation, grant 23-21-00175, https://rscf.ru/project/23-21-00175/

References

[1] Cyrus K Aidun and Jonathan R Clausen. Lattice-boltzmann method for complex flows. *Annual review of fluid mechanics*, 42:439–472, 2010.

[2] Eyvind Aker, Knut JØrgen MÅlØy, Alex Hansen, and G George Batrouni. A two-dimensional network simulator for two-phase flow in porous media. *Transport in porous media*, 32:163–186, 1998.

[3] GI Barenblatt, TW Patzek, and DB Silin. The mathematical model of nonequilibrium effects in water-oil displacement. *SPE journal*, 8(04):409–416, 2003.

[4] Grigory I Barenblatt, Iu P Zheltov, and IN Kochina. Basic concepts in the theory of seepage of homogeneous liquids in fissured rocks [strata]. *Journal of applied mathematics and mechanics*, 24(5):1286–1303, 1960.

[5] Maria C Bravo and Mariela Araujo. Analysis of the unconventional behavior of oil relative permeability during depletion tests of gas-saturated heavy oils. *International journal of multiphase flow*, 34(5):447–460, 2008.

[6] Jing-Den Chen and David Wilkinson. Pore-scale viscous fingering in porous media. *Physical review letters*, 55(18):1892, 1985.

[7] Shiyi Chen and Gary D Doolen. Lattice boltzmann method for fluid flows. *Annual review of fluid mechanics*, 30(1):329–364, 1998.

[8] I Fatt. The network model of porous media. 3. dynamic properties of networks with tube radius distribution. *Transactions of the American institute of mining and metallurgical engineers*, 207(7):164–181, 1956.

[9] Yanbin Gong. *Dynamic Pore Network Modeling of Two-Phase Flow and Solute Transport in Disordered Porous Media and Rough-Walled Fractures*. University of Wyoming, 2021.

[10] S Majid Hassanizadeh. Continuum description of thermodynamic processes in porous media: Fundamentals and applications. *Modeling Coupled Phenomena in Saturated Porous Materials*, pages 179–223, 2004.

[11] S Majid Hassanizadeh, Michael A Celia, and Helge K Dahle. Dynamic effect in the capillary pressure–saturation relationship and its impacts on unsaturated flow. *Vadose Zone Journal*, 1(1):38–57, 2002.

[12] S Majid Hassanizadeh and William G Gray. High velocity flow in porous media. *Transport in porous media*, 2:521–531, 1987.

[13] S Majid Hassanizadeh and William G Gray. Mechanics and thermodynamics of multiphase flow in porous media including interphase boundaries. *Advances in water resources*, 13(4):169–186, 1990.

[14] S Majid Hassanizadeh and William G Gray. Thermodynamic basis of capillary pressure in porous media. *Water resources research*, 29(10):3389–3405, 1993.

[15] M King Hubbert. Darcy's law and the field equations of the flow of underground fluids. *Transactions of the AIME*, 207(01):222–239, 1956.

[16] V Joekar-Niasar, S Majid Hassanizadeh, and HK Dahle. Non-equilibrium effects in capillarity and interfacial area in two-phase flow: dynamic pore-network modelling. *Journal of fluid mechanics*, 655:38–71, 2010.

[17] PR King. The fractal nature of viscous fingering in porous media. *Journal of Physics A: Mathematical and General*, 20(8):L529, 1987.

[18] VI Kondaurov. The thermodynamically consistent equations of a thermoelastic saturated porous medium. *Journal of applied mathematics and mechanics*, 71(4):562–579, 2007.

[19] VI Kondaurov. A non-equilibrium model of a porous medium saturated with immiscible fluids. *Journal of Applied Mathematics and Mechanics*, 73(1):88–102, 2009.

[20] Andrey Konyukhov, Leonid Pankratov, and Anton Voloshin. The homogenized kondaurov type non-equilibrium model of two-phase flow in multiscale non-homogeneous media. *Physica Scripta*, 94(5):054002, 2019.

[21] N Labed, L Bennamoun, and JP Fohr. Experimental study of two-phase flow in porous media with measurement of relative permeability. *Fluid Dyn. Mater. Process*, 8(4):423–436, 2012.

[22] Stephen B Pope and Stephen B Pope. *Turbulent flows*. Cambridge university press, 2000.

[23] Harris Sajjad Rabbani. *Pore-scale investigation of wettability effects on two-phase flow in porous media*. The University of Manchester (United Kingdom), 2018.

[24] Amir Raoof and S Majid Hassanizadeh. A new method for generating pore-network models of porous media. *Transport in porous media*, 81:391–407, 2010.

[25] Santanu Sinha, Andrew T Bender, Matthew Danczyk, Kayla Keepseagle, Cody A Prather, Joshua M Bray, Linn W Thrane, Joseph D Seymour, Sarah L Codd, and Alex Hansen. Effective rheology of two-phase flow in three-dimensional porous media: experiment and simulation. *Transport in porous media*, 119:77–94, 2017.

[26] Cameron Tropea, Alexander L Yarin, John F Foss, et al. *Springer handbook of experimental fluid mechanics*, volume 1. Springer, 2007.

[27] Grétar Tryggvason, Bernard Bunner, Asghar Esmaeeli, Damir Juric, N Al-Rawahi, W Tauber, J Han, S Nas, and Y-J Jan. A front-tracking method for the computations of multiphase flow. *Journal of computational physics*, 169(2):708–759, 2001.

[28] Markus Uhlmann. An immersed boundary method with direct forcing for the simulation of particulate flows. *Journal of computational physics*, 209(2):448–476, 2005.

[29] Per H Valvatne and Martin J Blunt. Predictive pore-scale modeling of two-phase flow in mixed wet media. *Water resources research*, 40(7), 2004.

[30] Edward W Washburn. The dynamics of capillary flow. *Physical review*, 17(3):273, 1921.

[31] Wikipedia. Capillary action — Wikipedia, the free encyclopedia. `http://en.wikipedia.org/w/index.php?title=Capillary%20action&oldid=1155129318`, 2023. [Online; accessed 19-June-2023].

[32] Wahyu Perdana Yudistiawan, Sang Kyu Kwak, and Santosh Ansumali. Higher order galilean invariant lattice boltzmann model. In *The 6th International Conference for Mesoscopic Methods in Engineering and Science*, page 28, 2009.